Polycyclic Aromatic Hydrocarbons

International Edition: DOI: 10.1002/anie.201502977
German Edition: DOI: 10.1002/ange.201502977

Boron-Containing Polycyclic Aromatic Hydrocarbons: Facile Synthesis of Stable, Redox-Active Luminophores**

*Valentin M. Hertz, Michael Bolte, Hans-Wolfram Lerner, and Matthias Wagner**

Abstract: *Herein we show that replacing the two meso carbon atoms of the polycyclic aromatic hydrocarbon (PAH) bisanthene by boron atoms transforms a near-infrared dye into an efficient blue luminophore. This observation impressively illustrates the impact of boron doping on the frontier orbitals of PAHs. To take full advantage of this tool for the targeted design of organic electronic materials, the underlying structure–property relationships need to be further elucidated. We therefore developed a modular synthesis sequence based on a Peterson olefination, a stilbene-type photocyclization, and an Si–B exchange reaction to substantially broaden the palette of accessible polycyclic aromatic organoboranes and to permit a direct comparison with their PAH congeners.*

The incorporation of main-group elements into π-conjugated organic systems leads to novel compounds with remarkable optoelectronic properties. Careful selection of the non-carbon dopant provides a valuable set screw to tune the frontier orbital energy levels and, in turn, the UV/Vis absorption/emission characteristics as well as the charge-transport and charge-storage capacities of the resulting materials.[1]

Boron-containing π-electron systems entered the center stage of organic materials development only two decades ago and since then have attracted increasing attention.[2] The vacant p_z orbital of a three-coordinate boron atom readily interacts with an adjacent π-electron cloud. As a result, conjugated organoboranes tend to be luminescent and to acquire an electron-accepting/conducting character. Consequently, they lead to n-type materials, which are in great demand but more difficult to obtain than their p-type complements.[3] Three different classes of arylboranes have to be distinguished (Figure 1):[2] In type **A** compounds, the boron atom is attached to the π system by only one bond and sterically protected by two bulky substituents such as the mesityl (Mes) group. In type **B** compounds, two boron valencies are employed to incorporate the atoms into the conjugation path. Finally, in type **C** compounds the boron atom is connected to the organic framework through all three of its valencies.[4]

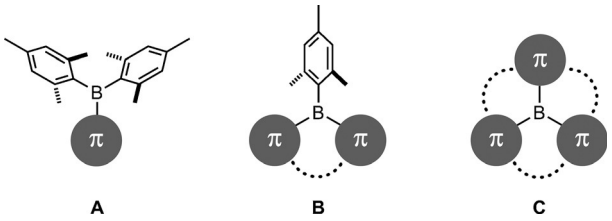

Figure 1. Three fundamental classes of stable arylboranes.

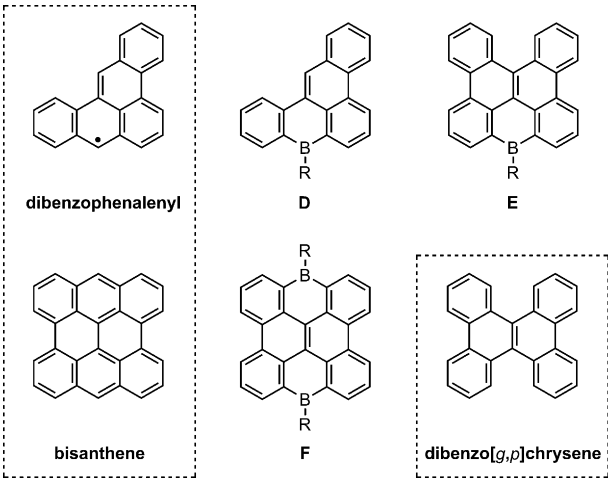

Figure 2. Three structurally related boron-doped PAHs in comparison to their all-carbon congeners.

Our group has developed various luminophores based on the 9,10-dihydro-9,10-diboraanthracene building block.[5] Moreover, we succeeded in the synthesis of a dianionic dibenzo[*g*,*p*]chrysene (cf. Figure 2) derivative with a central B=B bond.[6] For the next stage, we are aiming at an extension of the π-conjugated frameworks. The new target compound **F** (Figure 2) can be regarded as a 7,14-dihydro-7,14-diborabisanthene and consequently as stretched version of the 9,10-dihydro-9,10-diboraanthracene scaffold. Alternatively, one may view **F** as a doubly boron-bridged dibenzo[*g*,*p*]chrysene. Bisanthene is usually classified as a closed-shell species, but quantum-chemical calculations indicate a non-negligible degree (7–12%) of radicaloid character at its zigzag edges.[7] As a consequence, parent bisanthene is highly reactive toward molecular oxygen.[8] To achieve long-term air stability, sterically demanding substituents have to be attached at the *meso* positions C-7 and C-14.

[*] M. Sc. V. M. Hertz, Dr. M. Bolte, Dr. H.-W. Lerner, Prof. Dr. M. Wagner
Institut für Anorganische Chemie
Goethe-Universität Frankfurt
Max-von-Laue-Strasse 7, 60438 Frankfurt (Main) (Germany)
E-mail: Matthias.Wagner@chemie.uni-frankfurt.de

[**] We thank Prof. M. C. Holthausen and Prof. H. F. Bettinger for helpful discussions.

Supporting information for this article (including all experimental procedures together with further crystallographic and spectroscopic details) is available on the WWW under http://dx.doi.org/10.1002/anie.201502977.

 © 2015 Wiley-VCH Verlag GmbH & Co. KGaA, Weinheim

The number of *meso*-derivatized bisanthenes is very limited.[9] Among them, the 7,14-bisanthenequinones are particularly important to qualitatively predict the effect of boron doping: Oxidation of the blue-colored near-infrared (NIR) dye bisanthene to its yellow quinone results in a pronounced hypsochromic shift of the absorption and emission maxima (cf. Supporting Information (SI), Table S1).[8,10] Yet, a solution of 7,14-bisanthenequinone in H_2SO_4 adopts a violet color with absorption and emission wavelengths in between those of bisanthene (in C_6H_6) and 7,14-bisanthenequinone (in CH_2Cl_2).[10] A higher solvent acidity obviously correlates with an increasing degree of carbenium-ion character at the *meso* positions of the quinone. Given the isoelectronic relationship between the boron atom and the carbenium ion, it will be revealing to see how the optoelectronic properties of type **F** compounds compare to those of 7,14-bisanthenequinones, bisanthenes, and dibenzo[*g*,*p*]chrysenes (Figure 2).

Herein we disclose a facile synthesis of the boron-containing, type **F** bisanthene **12**, which proved to be an air- and water-stable blue luminophore. The modular synthesis protocol developed for **F** also provides convenient access to various other boron-doped PAHs (Figure 2), such as singly bridged dibenzo[*g*,*p*]chrysenes (cf. **E**) and boraphenalenes[11] (cf. **D**).

The basic structures **D**, **E**, and **F** were modified by introduction of solubilizing *t*Bu substituents and sterically protecting mesityl groups (cf. **8a–e**, **9**, and **12**). For reasons of efficiency, we aimed at a highly variable approach: All noncommercial building blocks, **3**–**5**,[12] are accessible from the readily available starting material **1** (Scheme 1), and all synthesis sequences are based on the same key transformations, i.e., a Peterson olefination,[13] a stilbene-type photocyclization,[14] and an Si–B exchange[15] reaction. The modularity of the general synthesis strategy is illustrated in Scheme 2; synthesis details will be exemplarily described for compound **12** (Scheme 3).

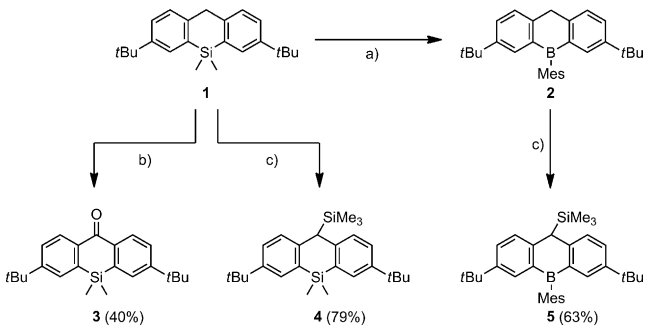

Scheme 1. Yields are given relative to **1**. Reagents and conditions: a) 1. excess neat BBr_3, RT; 2. 1.5 equiv MesMgBr, toluene/THF, RT; b) 1 equiv CrO_3, AcOH, 70 °C; c) 1. 1 equiv *n*BuLi, Et_2O, 0 °C; 2. 1.5 equiv Me_3SiCl, Et_2O, 0 °C.

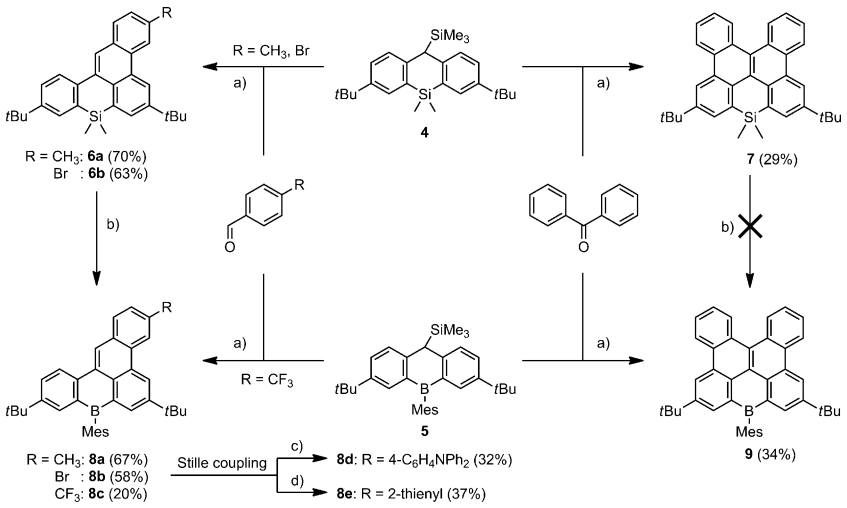

Scheme 2. Yields are given relative to **4** or **5**. Reagents and conditions: a) 1. 1 equiv *n*BuLi, Et_2O, 0 °C; 2. 1 equiv carbonyl compound, Et_2O, 0 °C; 3. UV irradiation (Hg medium-pressure lamp; I_2, propylene oxide), toluene or cyclohexane, RT; b) 1. excess neat BBr_3, 0 °C to 50 °C; 2. 2 equiv MesMgBr, toluene/THF, 0 °C; c) 2.5 equiv 4-*n*$Bu_3Sn(C_6H_4)NPh_2$, [$Pd(PtBu_3)_2$] (5 mol%), toluene, 100 °C; d) 2 equiv 2-*n*$Bu_3Sn(C_4H_3S)$, [$Pd(PtBu_3)_2$] (5 mol%), toluene, 90 °C.

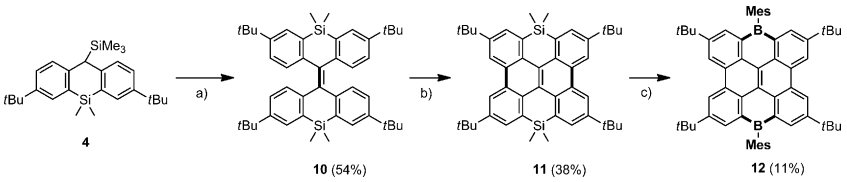

Scheme 3. Yields are given relative to **4**. Reagents and conditions: a) 1. 1 equiv *n*BuLi, THF, −78 °C to RT; 2. 1 equiv **3**, THF, −78 °C to RT; b) UV irradiation (Hg medium-pressure lamp; I_2, propylene oxide), toluene, RT; c) 1. excess neat BBr_3, 200 °C, 4 days; 2. 3 equiv MesMgBr, toluene/THF, 0 °C.

The Peterson olefination furnished the challenging, sterically encumbered olefin **10** (Scheme 3) in 54% yield. Furthermore, it allows for the synthesis of unsymmetrically substituted olefins, which are required for the preparation of **8a–c** and **9** from **4**/**5** and commercial carbonyl compounds (Scheme 2). The subsequent dehydrogenative C–C coupling step via a twofold photocyclization of **10** to **11** is compatible with acid-sensitive, silicon-containing species. It even benefits from the heteroatom bridges, as they assist in the appropriate preorganization of the *peri* hydrogen atoms (Scheme 3). The Si–B exchange was the most demanding hurdle on the way to the target compound **12**, because of the extraordinarily rigid molecular scaffold. For optimal results, **11** had to be suspended in neat BBr_3 and heated to 200 °C for 4 days in a sealed glass ampoule. In contrast, the Si–B exchange on **6a**,**b** proceeds quantitatively already near room temperature (Scheme 2). Compound **7** did neither react at ambient temperature, nor is it compatible with forcing conditions. Since our synthesis approach allows for the introduction of the boron atom already at an earlier stage, **9** finally became

 © 2015 Wiley-VCH Verlag GmbH & Co. KGaA, Weinheim

available from benzophenone and the 9,10-dihydro-9-boraanthracene **5**. Besides its role in the synthesis of **9**, compound **5** also proved useful for the synthesis of otherwise inaccessible derivatives, such as the CF_3-substituted **8c**. The bromo derivative **8b** undergoes Stille-type coupling reactions at the boron-containing scaffold to create bipolar[16] molecules such as **8d** (R = 4-$C_6H_4NPh_2$) and **8e** (R = 2-thienyl; Scheme 2). All the arylborane products are long-term stable toward air and moisture.

The molecular structures of **8a**, **9**, and **12** were determined by X-ray crystallography (Figure 3).[17] Compound **8a** is

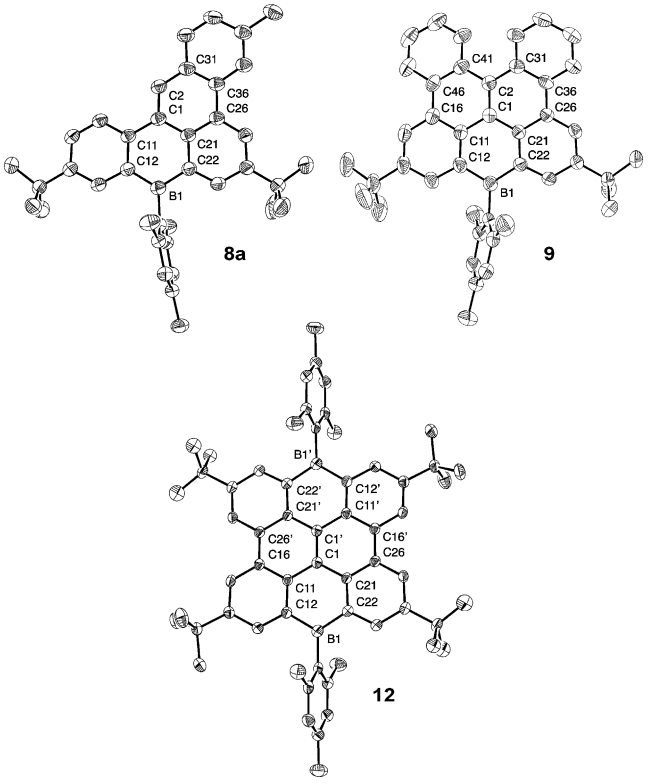

Figure 3. Molecular structures of **8a**, **9**, and **12** in the solid state. Displacement ellipsoids are drawn at the 50% probability level.

almost perfectly planar. Annulation of two benzene rings leads to a pronounced helical twist in **9** (cf. SI). The introduction of the second BMes bridge, in turn, alleviates the twist and leads to a largely planar C_i-symmetric structure **12.**

The ^1H and $^{13}C\{^1H\}$ NMR resonances of all target compounds and intermediates were assigned and are fully consistent with the proposed molecular structures. Typical for triarylboranes, the $^{11}B\{^1H\}$ signals are broadened and their chemical shift values fall in the narrow range between $\delta(^{11}B) = 65$ ppm and 70 ppm. Upon photocyclization, all PAH proton signals experience significant downfield shifts, especially in the newly formed bay regions [cf. **10**→**11**: $\delta(^1H) = 6.90 \rightarrow 8.80$ ppm (bay region), $\delta(^1H) = 7.55 \rightarrow 8.02$ ppm (zigzag region)].

The cyclic voltammogram (CV) of parent dibenzo[*g*,*p*]chrysene in CH_2Cl_2 shows several ill-defined features in the oxidizing region; no reduction potentials have been reported.[18] In comparison, the planarized, doubly Si-bridged **11** (cf. Table 1) undergoes reversible oxidation at $E_{1/2} = 0.81$ V (vs. FcH/FcH^+; CH_2Cl_2); no reduction events are observed up to the limit of the solvent's potential window at −2.3 V. The boron-bridged dibenzo[*g*,*p*]chrysenes show an increased redox activity: Compound **9** gives rise to two reversible redox events at $E_{1/2} = 1.00$ V and −2.01 V, whereas the CV of **12** is characterized by three reversible one-electron transitions at $E_{1/2} = 1.09$ V, −1.85 V, and −2.14 V. For 7,14-di(mesityl)bisanthene, the all-carbon congener of **12**,[19] half-wave potentials have been reported at 0.65 V, 0.02 V, and −1.66 V, together with a peak potential at −2.19 V, the latter indicating an irreversible electron transfer. Thus, we find the boron-containing compound **12**, which is isoelectronic to the 7,14-di(mesityl)bisanthene dication, harder to oxidize by 1 V than 7,14-di(mesityl)bisanthene itself. The reduction potentials of both compounds, however, are rather similar (Table 1). Each of the investigated type **D** compounds gives rise to one reduction wave between $E_{1/2} = -2.0$ V and −2.2 V. In addition, the methyl-substituted derivative **8a** can be reversibly oxidized at a potential value of $E_{1/2} = 0.99$ V; the bipolar species **8d** undergoes two redox transitions at $E_{1/2} =$ 0.94 V and 0.48 V. The CF_3- and 2-thienyl-substituted species do not show interpretable oxidation waves.

The longest-wavelength absorptions of all boron-doped PAHs **8a–e**, **9**, and **12** fall in the range between $\lambda_{max} = 400$ nm and 450 nm (Table 1). As a result of the rigid molecular frameworks, the Stokes shifts are generally small and a vibrational fine structure is resolved in the emission spectra (cf. the SI for plots of all the absorption and emission spectra).[20] Relative to dibenzo[*g*,*p*]chrysene ($\lambda_{em} = 395$ nm),[21] the emission maxima of **9** and **12** are bathochromically shifted to $\lambda_{em} =$ 439 nm and 449 nm, respectively (Figure 4; Table 1). Most

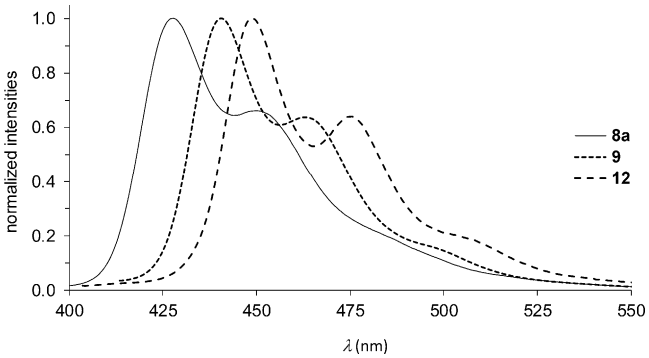

Figure 4. Emission spectra of **8a**, **9**, and **12** in cyclohexane.

importantly, the boron-containing molecules exhibit drastically improved photoluminescence quantum yields (**9**: $\Phi_{PL} =$ 70%, **12**: $\Phi_{PL} = 78\%$) compared to that of dibenzo[*g*,*p*]chrysene ($\Phi_{PL} = 19\%$).[18] The planarized silicon-bridged compounds are again only moderately efficient luminophores (**7**: $\Phi_{PL} = 20\%$, **11**: $\Phi_{PL} = 35\%$). Considering these observations, we attribute the superior quantum yield of the boron-doped PAHs mainly to the specific electronic influence of the boron atoms with their π-conjugated p_z orbitals (and less so to

 © 2015 Wiley-VCH Verlag GmbH & Co. KGaA, Weinheim

Table 1: Photophysical and electrochemical data of selected arylboranes and compounds used for comparison. Unless noted otherwise, all optical measurements were performed in C_6H_{12}.

Cmpd	λ_{abs} [nm] (ε [$M^{-1}cm^{-1}$])	λ_{onset} [nm][a]	λ_{ex} [nm]	λ_{em} [nm]	Φ_{PL} [%][b]	Stokes shift [cm^{-1}][c]	E_{HOMO}/E_{LUMO} [eV][d]	$E_{1/2}$ [V]	E_G^{CV} [eV][e]	E_G^{opt} [eV][f]
8a	395 (18000) 416 (30000)	428	375	428 450	88	674	−5.79/−2.63	−2.17 0.99	3.16	2.90
8c	381 (21000) 401 (30000)	414	370	412 434	79	666	–/−2.79	−2.01	–	3.00
8d	391 (22000) 433 (40000)	466	410	471 498	92	1863	−5.28/−2.70	−2.10 0.48 0.94	2.58	2.66
8e	389 (18000) 411 (23000) 429 (32000)	447	400	447 473	73	1960	–/−2.71	−2.09	–	2.77
9	407 (14000) 429 (22000)	441	400	439 465	70	531	−5.80/−2.79	−2.01 1.00	3.01	2.81
11	347 (18000) 361 (18000)	391	345	390 408	35	2060	−5.61/–	0.81	–	3.17
12	418 (31000) 432 (42000) 442 (34000)	452	390	449 475	78	353	−5.89/−2.95	−2.14 −1.85 1.09	2.94	2.74
bisanthene[g]	625 685	715	–	705	–	415	−4.82/−3.14	−1.66 0.02 0.65	1.68	1.73

[a] Each onset wavelength (λ_{onset}) was determined by constructing a tangent at the point of inflection of the bathochromic slope of the most red-shifted absorption maximum. [b] Quantum yields were determined by using a calibrated integrating sphere. [c] Stokes shifts represent the difference between each longest wavelength absorption maximum and the corresponding shortest wavelength emission maximum. [d] $E_{HOMO} = -4.8\ eV - E_{1/2}^{Ox1}$, $E_{LUMO} = -4.8\ eV - E_{1/2}^{Red1}$ ($FcH/FcH^+ = -4.8$ eV vs vacuum level). [e] Electrochemically determined band gap. [f] Optical band gap $E_G^{opt} = 1240/\lambda_{onset}$. [g] 7,14-di(mesityl)bisanthene.[19]

the planarizing effect of the heteroatom bridges). The most efficient luminophores are found among the type **D** compounds (Table 1), with $\Phi_{PL} = 88\%$ for **8a** and 92% for the bipolar **8d**. Compared to **8a**, which carries a largely innocent CH_3 group, the electron-rich amine substituent in **8d** leads to a significant bathochromic shift of λ_{em} from 428 nm to 471 nm. As expected, only the bipolar compound exhibits a pronounced solvatochromism (see SI for details).

In terms of HOMO–LUMO energy differences (Table 1), the boron-containing periacene **12** ($E_g^{opt} = 2.74$ eV) adopts a position between its all-carbon relatives dibenzo[*g*,*p*]chrysene[21] (larger gap; $E_g^{opt} = 3.13$ eV) and 7,14-di(mesityl)bisanthene[19] (smaller gap; $E_g^{opt} = 1.73$ eV). Compound **12** stands out from the triarylborane family for its high photoluminescence quantum yield in combination with the capability to undergo reversible redox transitions both in the cathodic and anodic regime. The highly modular synthesis strategy developed for **12** also paves the way for the preparation of numerous other polycyclic conjugated boranes. The foundation is laid for a systematic assessment of structure–property relationships and, in turn, the targeted optimization of boron-doped nanographene materials.

Keywords: boron · luminescence · organic electronics · organoboranes · polycyclic aromatic hydrocarbons

How to cite: *Angew. Chem. Int. Ed.* **2015**, *54*, 8800–8804
Angew. Chem. **2015**, *127*, 8924–8928

[1] a) T. Baumgartner, R. Réau, *Chem. Rev.* **2006**, *106*, 4681–4727; b) X. He, T. Baumgartner, *RSC Adv.* **2013**, *3*, 11334–11350.

[2] a) C. D. Entwistle, T. B. Marder, *Angew. Chem. Int. Ed.* **2002**, *41*, 2927–2931; *Angew. Chem.* **2002**, *114*, 3051–3056; b) S. Yamaguchi, A. Wakamiya, *Pure Appl. Chem.* **2006**, *78*, 1413–1424; c) F. Jäkle, *Chem. Rev.* **2010**, *110*, 3985–4022; d) Y.-L. Rao, H. Amarne, S. Wang, *Coord. Chem. Rev.* **2012**, *256*, 759–770; e) A. Lorbach, A. Hübner, M. Wagner, *Dalton Trans.* **2012**, *41*, 6048–6063.

[3] M. Stolar, T. Baumgartner, *Phys. Chem. Chem. Phys.* **2013**, *15*, 9007–9024.

[4] Selected examples: a) Z. Zhou, A. Wakamiya, T. Kushida, S. Yamaguchi, *J. Am. Chem. Soc.* **2012**, *134*, 4529–4532; b) C. Dou, S. Saito, K. Matsuo, I. Hisaki, S. Yamaguchi, *Angew. Chem. Int. Ed.* **2012**, *51*, 12206–12210; *Angew. Chem.* **2012**, *124*, 12372–12376.

[5] a) A. Lorbach, M. Bolte, H. Li, H.-W. Lerner, M. C. Holthausen, F. Jäkle, M. Wagner, *Angew. Chem. Int. Ed.* **2009**, *48*, 4584–4588; *Angew. Chem.* **2009**, *121*, 4654–4658; b) A. Lorbach, M. Bolte, H.-W. Lerner, M. Wagner, *Organometallics* **2010**, *29*, 5762–5765; c) C. Hoffend, F. Schödel, M. Bolte, H.-W. Lerner, M. Wagner, *Chem. Eur. J.* **2012**, *18*, 15394–15405; d) C. Reus, S. Weidlich, M. Bolte, H.-W. Lerner, M. Wagner, *J. Am. Chem. Soc.* **2013**, *135*, 12892–12907; e) C. Reus, F. Guo, A. John, M. Winhold, H.-W. Lerner, F. Jäkle, M. Wagner, *Macromolecules* **2014**, *47*, 3727–3735.

[6] A. Hübner, M. Bolte, H.-W. Lerner, M. Wagner, *Angew. Chem. Int. Ed.* **2014**, *53*, 10408–10411; *Angew. Chem.* **2014**, *126*, 10576–10579.

[7] a) A. Konishi, Y. Hirao, M. Nakano, A. Shimizu, E. Botek, B. Champagne, D. Shiomi, K. Sato, T. Takui, K. Matsumoto, H. Kurata, T. Kubo, *J. Am. Chem. Soc.* **2010**, *132*, 11021–11023; b) A. Shimizu, Y. Hirao, T. Kubo, M. Nakano, E. Botek, B. Champagne, *AIP Conf. Proc.* **2012**, *1504*, 399–405.

[8] S. M. Arabei, T. A. Pavich, *J. Appl. Spectrosc.* **2000**, *67*, 236–244.

[9] J. Li, K. Zhang, X. Zhang, K.-W. Huang, C. Chi, J. Wu, *J. Org. Chem.* **2010**, *75*, 856–863, and references therein.

 © 2015 Wiley-VCH Verlag GmbH & Co. KGaA, Weinheim

[10] U. Müller, V. Enkelmann, M. Adam, K. Müllen, *Chem. Ber.* **1993**, *126*, 1217 – 1225.
[11] J. M. Zoellner, R. W. Zoellner, *THEOCHEM* **2009**, *904*, 49 – 56.
[12] R. v. Veen, F. Bickelhaupt, *J. Organomet. Chem.* **1974**, *77*, 153 – 165.
[13] L. F. v. Staden, D. Gravestock, D. J. Ager, *Chem. Soc. Rev.* **2002**, *31*, 195 – 200.
[14] L. Liu, B. Yang, T. J. Katz, M. K. Poindexter, *J. Org. Chem.* **1991**, *56*, 3769 – 3775.
[15] a) A. Wakamiya, K. Mishima, K. Ekawa, S. Yamaguchi, *Chem. Commun.* **2008**, 579 – 581; b) A. Hübner, M. Diefenbach, M. Bolte, H.-W. Lerner, M. C. Holthausen, M. Wagner, *Angew. Chem. Int. Ed.* **2012**, *51*, 12514 – 12518; *Angew. Chem.* **2012**, *124*, 12682 – 12686; c) See Ref. [4a].
[16] H. Doi, M. Kinoshita, K. Okumoto, Y. Shirota, *Chem. Mater.* **2003**, *15*, 1080 – 1089.
[17] CCDC 1037642, CCDC 1037644, CCDC 1037645, CCDC 1037646, CCDC 1037647, CCDC 1037648, CCDC 1037649, CCDC 1037650, CCDC 1037651, CCDC 1037652, CCDC 1037653, CCDC 1037654, CCDC 1052209, and CCDC 1052210 contain the supplementary crystallographic data for this paper and can be obtained free of charge from The Cambridge Crystallographic Data Centre via www.ccdc.cam.ac.uk/data_request/cif..
[18] R. Chaudhuri, M.-Y. Hsu, C.-W. Li, C.-I. Wang, C.-J. Chen, C. K. Lai, L.-Y. Chen, S.-H. Liu, C.-C. Wu, R.-S. Liu, *Org. Lett.* **2008**, *10*, 3053 – 3056.
[19] A. Konishi, Y. Hirao, K. Matsumoto, H. Kurata, T. Kubo, *Chem. Lett.* **2013**, *42*, 592 – 594.
[20] Resolved maxima of the vibronic fine structures are compiled in Table 1 (see the SI for plots of the spectra). The λ_{em} values discussed in the main text refer to the most intense local maximum of each emission band.
[21] S. Hashimoto, T. Ikuta, K. Shiren, S. Nakatsuka, J. Ni, M. Nakamura, T. Hatakeyama, *Chem. Mater.* **2014**, *26*, 6265 – 6271.

Received: March 31, 2015
Published online: June 8, 2015

 © 2015 Wiley-VCH Verlag GmbH & Co. KGaA, Weinheim